LAWRENCE
LIVERMORE
NATIONAL
LABORATORY

UCRL-CONF-206835

THE USE OF MICROELECTRODES IN THE STUDY OF THE EFFECTS OF ELECTROLYTE COMPOSITION, POTENTIAL AND METALLURGICAL CONDITION ON NUCLEATION AND METASTABLE PITTING OF STAINLESS STEEL 316

G. O. Ilevbare, G. T. Burstein

September 27, 2004

206th Meeting of the Electrochemical Society
Honolulu, HI, United States
October 3, 2004 through October 8, 2004

THE USE OF MICROELECTRODES IN THE STUDY OF THE EFFECTS OF ELECTROLYTE COMPOSITION, POTENTIAL AND METALLURGICAL CONDITION ON NUCLEATION AND METASTABLE PITTING OF STAINLESS STEEL 316

G. O. ILEVBARE* AND G.T. BURSTEIN

Department of materials Science and Metallurgy, Pembroke Street, University of Cambridge, Cambridge, UK

*Present Address: Lawrence Livermore National Laboratory, L-631, 7000 East Avenue, Livermore CA 94550, USA

ABSTRACT

The study of stainless steel 316 has been undertaken in electrolytes containing various concentrations of chloride (Cl^-) and perchlorate (ClO_4^-) ions. The concentration of Cl^- and ClO_4^- in these electrolytes varied between 0.025 and 0.1 M in a variety of combinations. Results showed that the total number of nucleation and metastable pitting events increased as [Cl^-] and potential increased. However, the percentage propagation rate of metastable pits from nucleations increased. The data also showed that the metallurgical condition of the specimen affected the number of nucleations and metastable pits generated

INTRODUCTION

The pitting potential is considered the minimum potential at which stable pitting occurs and can be autocatalytically sustained [1-5]. However, pitting corrosion in the form of nucleations and metastable pitting starts taking place at potentials far below the pitting potential [5-9]. Therefore, catastrophic pitting corrosion is limited to potentials at and above the pitting potential. Until relatively recently, very little attention has been paid to the precursor events of pitting which occur below the pitting potential. The process of pitting corrosion has been found to proceed via three consecutives steps namely: nucleation, metastable pitting and stable pitting [7-8].

Typically, relatively large electrodes are used in the study of pitting corrosion, many of which have focused on the measurement of the pitting potential. These large electrodes are usually not useful in the study of nucleations and metastable pitting events. This is because the passive currents generated on these large electrodes far exceed the currents generated by nucleations and metastable pits. The passive currents generated on standard electrodes used in pitting corrosion studies usually fall within 10^{-7} and 10^{-6}amps, while peak currents measured for nucleation and metastable pitting events have been in the region of 10^{-12} to 10^{-9} [5-10]. Consequently, very small electrodes (microelectrodes) which have a passive current density in the region of 10^{-12}amps have to be used for study in order to allow current signatures from nucleations and metastable pitting to be seen

above thee passive current. However, it is not always possible to measure pitting potentials on microelectrodes because they do not always pit due to a scarcity of viable sites suitable for sustaining stable pitting [9, 10].

Two of the most important factors that affect the onset of stable pitting are aggressive ion (e.g. Cl^-) concentration and applied potential. An increase in the applied potential and/or [Cl^-] increases the chances of generating stable pitting. This paper addresses the effect of these two factors on the nucleation and metastable pitting behavior of stainless steel. An additional interest is in how metallurgical factors influence these microevents.

EXPERIMENTAL METHOD

AISI 316 from two different sources were used in potentiostatic experiments performed in a two-electrode cell (150 cm^3) at a constant potential of 0.2, 0.3 and 0.5 V (SCE). From one source, pre-drawn 50μm diameter 316 wires (surface area: 2 x 10^{-5} cm^2; designated SS316GF) which had no sulphide inclusions 1 μm (detection limit of instrument) in diameter or larger detectable with SEM-EDX were used to fabricate microelectrodes. EDX analysis of SS316GF is reported in Table 1. The metal was not sensitized. Carbon was not analyzed for. From another source, microelectrodes were fabricated by electropolishing 0.1 x 0.1 x 18 cm portions of commercially available 0.1 cm thick AISI 316 plates (designated 316Com). Electropolishing in 10.5M H_3PO_4, between 55 and 60 ^oC, at cell voltage of 2.0V, was done to fabricate ~12 cm long wires with fairly circular cross sectional surface areas of between 3.18 and 3.9 x $10^{-4}cm^2$. The composition 316Com is shown in Table 2. Circular sulphide inclusions (probably MnS, FeS, or CrS) measuring 1 to 3 μm in diameter and less than 1 μm thick were detected on the surface by EDX. No secondary phase precipitates were detected. The metal was not sensitized.

A silver/silver chloride (Ag/AgC1) was the combined reference and counter electrode. Currents between 1 and 350 pA were measured through a current amplifier at a gain of 10^{10} VA^{-1}. Potential was applied through the voltage bias system of the current amplifier. The current output was fed through a digital voltmeter (DVM) into a computer. Data acquisition took for 2370 s at 13.5 Hz, giving 32 000 data points stored in 16 segments of 2000 data points every 148 s. Housing the cell and the current amplifier in two separate Faraday cages reduced the noise level. Polarization started immediately the electrode was introduced into the electrolyte. The electrolytes (0.025M HCl + 0.075M $HClO_4$, 0.05M HCl + 0.05M $HClO_4$, 0.075M HCl + 0.025M $HClO_4$, and 0.1MHCl) were deaerated for 1 hour before and throughout experimentation. All electrolytes had a pH of 1.0. $HClO_4$ acted as a supporting electrolyte, allowing solution pH to be maintained at 1.0 while [Cl^-] was varied. At least 10 repeat experiments were carried out for each metal/solution combination examined to provide a statistical basis for the results. Electrode surfaces were finished with 1200 grit silicon carbide (SiC) paper. All experiments were carried out at an ambient temperature of 17 ± 3 °C

Analyses of Events

A threshold value of 1.6pA was used for analyses to obtain the frequency of nucleation, metastable pitting, and the size (height) of events when SS316GF was studied (effect of [Cl^-] and E). However a threshold value of 4.0 pA was used when SS616GF

was compared with 316Com due to the nosier background current of 316Com. The method for the determination of the threshold value for analyses is reported in detail elsewhere [9]. All error bars are at a 95% confidence level.

EXPERIMENTAL RESULTS

Figure 1 shows a current transient obtained from SS316GF in 0.1M HCl at 0.2V (SCE). The background current decayed with time. Superimposed on the background current are many intermittent anodic current spikes. These anodic current spikes are either nucleation or metastable pitting events since no stable pitting occurred. The current was user-limited to 350pA to obtain a good resolution of small nucleation events, hence the initial ~500 s period of current overload (Figure 1). Peak currents in this region of overload lie between 10 and 100nA. The observed frequency and peak height (size) of events is highest early in the experiment. A more detailed description of nucleations and metastable pits can be found elsewhere [5, 7-9]. Nucleations show a fast current rise and a fast but relatively gentler fall (Figure 2). Nucleation represents the rupture and repassivation of the oxide film, and occurs extremely quickly [7-9]. Metastable pits are a result of metal dissolution and hence pit propagation. They exhibit a stepwise current rise from background followed by an abrupt current jump and then a fall in current to background level [5]. Metastable pit transients are always preceded by a nucleation event [9]. Nucleation therefore represents the birth of a pit. The abrupt repassivation represents the death of the pit; it is always preceded by a sharp current increase.

Chloride Concentration Dependence

The semi-logarithmic plot in Figure 3 shows that the average frequency per cm^2 of nucleations decays exponentially with time. The frequency of nucleations increases as $[Cl^-]$ increases. The logarithmic plot of the average frequency per unit area (cm^2) of these events as a function of time fits a straight line as expected from equation [1]:

$$\lambda = \lambda_o \exp\left(-\frac{t}{\tau}\right) \qquad [1]$$

And hence

$$N_o = \lambda_o \tau \qquad [2]$$

Where $\boldsymbol{\lambda_o}$ is the initial frequency of events per cm^2, $\boldsymbol{\lambda}$ the frequency (rate) of nucleation, t is time in seconds, τ is the time constant and $\mathbf{N_o}$ is the total number of nucleations available. The average frequency was calculated from 15 runs for all the electrolytes except 0.025M HCl + 0.075M $HClO_4$ which was from 19 runs. Each point was plotted at the mid-point of the time interval (148 s) it represents. The error bars are at a 95% confidence level. Values for $\boldsymbol{\lambda_o}$, $\boldsymbol{\tau}$ and $\mathbf{N_o}$, were obtained from regression analyses (Table 3).

Figure 4 shows the average frequency per cm^2 of metastable pitting as a function of time. The data in Figure 4 was generated simultaneously from the same runs as the

average frequencies of nucleations were generated. Very few metastable pits occurred during the experiments resulting in a number of segments having no metastable pits occurring. The vertical axes of the graphs in Figure 4 have been broken to incorporate a linear scale to show the zero values otherwise impossible to show on the logarithmic scale. The regression lines on the graph are not therefore as accurate as those shown in Figure 3. However, the data also tend to show an exponential decay of the frequency with time. The values of τ and $\mathbf{N_o}$ for metastable pits increase roughly with increase in $[Cl^-]$. This shows an increase in propensity to generate metastable pits as $[Cl^-]$ increases (Table 3). The percentage of nucleations which proceeded to become metastable pits (from $\mathbf{N_o}$) were 20, 8.1, 9.0, and 3.1% for SS316GF in 0.025 M HCl + 0.075 M $HClO_4$, 0.05 M HCl + 0.05 M $HClO_4$, 0.075 M HCl + 0.025 M $HClO_4$ and 0.1 M HCl respectively (Figure 5).

The peak current (height) distribution of nucleation events is described in Figure 6. All the peaks in the distribution are between 1.6 and 350pA (current limit). Events smaller than 1.6pA if present were obscured by the background noise. Nucleations larger than 350pA although present, usually occurred during the first 500s of the experiment but were truncated of by the current limit. These events were few relative to the total number of nucleations that occurred. The height of nucleation events was grouped logarithmically using $^1/_3$-decade intervals. The groups include **A: 1.6 - 3.4 pA, B: 3.4 - 7.4 pA, C: 7.4 - 16 pA, D: 16 - 34.5 pA, E: 34.5 - 74.3 pA, F: 74.3 - 160 pA and G: >160.** The distribution of the peak height of events was not significantly affect by $[Cl^-]$. There is a consistent exponential decay in the number of nucleations with increase in logarithmic current range for the four sets of data presented.

The Effect of Applied Potential (**E**)

The effect of applied potential on nucleations and metastable pitting was examined on SS316GF in 0.025 M HCl + 0.075 M $HClO_4$ at 0.2, 0.3 and 0.5 V. Figure 7 compares the average frequencies of nucleations per cm^2 at 0.2 and 0.5V(SCE) and shows that there is an increase in the frequency as potential increases. These are the averages from 19 and 15 runs at 0.2 and 0.5V(SCE) respectively. There is an exponential decay of nucleations (Figure 7) and metastable pits (not shown) at all potentials. For nucleations, as potential increases, τ is unchanged while λ_o and $\mathbf{N_o}$ increase implying that τ is unaffected by **E (**Table 4**)**. For metastable pits, τ and $\mathbf{N_o}$ increased while λ_o remained constant, implying that **E** does not affect the rate of metastable pitting. However, Table 4 shows that the percentage of nucleations, which propagated into metastable pits, remained low, at 20, 8 and 16% for 0.2, 0.3 and 0.5V(SCE) respectively. These values suggest that the percentage of events, which propagated into metastable pits, did not change.

Figure 8 shows the height distribution of the nucleation events at different **E**. The current intervals are also $^1/_3$-decade intervals. There is an exponential decay in the number of events as the current range increases. Figure 8 suggests that **E** does not significantly change the size distribution of events nucleated.

Metallurgical Effects

SS316GF and SS316Com were compared in 0.025M HCl + 0.075M $HClO_4$ at 0.2V(SCE). The characteristics of the current transients of SS316Com are similar in all respects to those of SS316GF described in Figure 1. However, the decay of background

current to the level attained by SS316GF took a longer time. In all runs, the background current from 316Com was noisier compared with SS316GF. This was probably a result of the larger surface area of 316Com electrodes employed. Events also continued to occur for a longer duration, thus experiments were continued for much longer (11850 s) on 316Com.

Figures 9 and 10 show that the average frequencies of nucleation and metastable pitting per cm^2 on SS316GF and 316Com decayed exponentially as a function of time, but decayed at different rates. For 316Com, each data point represents the average frequency of events in 592 s. These are the averages from 10 and 19 runs for 316Com and SS316GF respectively. The values of $\boldsymbol{\lambda_o}$ and $\mathbf{N_o}$ are higher for SS316GF showing that more nucleations and metastable pits occurred and did so at a faster rate on SS316GF than on 316Com (Table 5). The time constant, $\boldsymbol{\tau}$, was longer on 316Com, showing that it took a longer time for the events to occur (Table 5). The percentage of nucleations that propagated into metastable pits was found to be 6.67% for 316Com and 35.48% for SS316GF, making it five times more likely that a metastable pit would occur on SS316GF than on 316Com (Table 5).

The height of nucleations is grouped logarithmically using $^1/_3$-decade intervals in Figure 11: **A: 4.0 - 8.6pA, B: 8.6 - 18.6pA, C: 18.6 - 40.0pA, D: 40.0 - 86.2pA, E: 86.2-185.7pA, and F: >185.7**. There is an exponential decay in the number of nucleations as the current range increases for 316Com but not on SS316GF. For SS316GF, this (no observed decay) is a result of using a threshold value of 4.0pA. Figure 6 shows that when the events between 1.6 and 3.9pA are included in the analysis for SS316GF, the decay in the number of nucleations is also exponential in nature. The percentage of nucleations is similar for both metals in ranges **B** and **C**. Thence SS316GF shows a larger proportion of events than 316Com in ranges **D**, **E** and **F** at the expense of events in range **A**.

DISCUSSION

The kinetics associated with the current decay in nucleations is consistent with classical repassivation kinetics of a freshly exposed metal surface [9, 11-13]. It is expected that little or no dissolution of metal occurs in nucleations as this would cause a deviation from classical repassivation kinetics. Brief metal dissolution takes place when metastable pits occur [5, 6]. Current from metastable pit growth is approximately proportional to t^2 and thus maintains a fairly constant current density as the pit grows [5].

A possible mechanism to explain the phenomenon of nucleation is by a field-driven migration of Cl^- ions across the oxide film probably occurring in parallel with oxide ion migration, the latter causing passivation by oxide film growth. On arriving at the oxide film/metal surface, formation of the metal chloride takes place. Since the molar volume of the metal chloride is much larger than that of the metal or the metal oxide [14], an internal pressure quickly builds up which eventually ruptures the oxide film on attainment of a critical volume, which exerts enough pressure to cause rupture. The critical volume would depend on the mechanical properties of the oxide film at the site and the geometry of the inclusion at the site.

In this mechanism, the process is localized because the weakest parts of the oxide film usually associated with inclusions are preferentially penetrated by Cl^- ions and the underlying inclusions are very quickly dissolved. The imperfections in the portion of the oxide film that cover these sites [15, 16] make the migration of Cl^- ions possible at these sites. The exponential decay of the rate of nucleation with time portrayed in Figures 3, 7 and 9 show that sites of pit nucleation are exhausted with time when exposed to aggressive environments.

It is expected that the total number of nucleations ($\mathbf{N_o}$) bear a relationship to the number of inclusions on the surface of the metal. However it is unlikely that the number of nucleactions equal the number of inclusions on the metal surface for a given set of condition ($[Cl^-]$, **E**), since this would imply that each nucleation results in the removal of an inclusion. This implies that more than one nucleation could occur on a single inclusion before the site is exhausted (if a metastable pit does not occur).

The increase in initial frequency of pit nucleation ($\boldsymbol{\lambda_o}$) with $[Cl^-]$ and **E** is consistent with the fact that passivity is less stable and the metal is more susceptible to pitting as $[Cl^-]$ and **E** increase. The increase in $\boldsymbol{\lambda_o}$ with $[Cl^-]$ may be explained under the proposed mechanism of nucleation as follows. Assuming a critical volume of metal chloride is required to cause the rupture of the oxide film at a particular site, and bearing in mind that the average number of Cl^- ions per unit volume increases with concentration, under the same field strength, it is expected that at higher $[Cl^-]$, the amount of Cl^- ions required for the formation of the critical volume of metal chloride necessary for film rupture will be attained faster. This is because more Cl^- ions will migrate through the film per unit time and hence a higher $\boldsymbol{\lambda_o}$ is realized. Increasing **E** increases the driving force on the Cl^- ions so that they migrate through the oxide film and accumulate faster. The result is that at constant $[Cl^-]$ the critical amount of ions required to cause film rupture is attained faster hence the increase in $\boldsymbol{\lambda_o}$ with **E**.

The increase in the time constant $\boldsymbol{\tau}$, and the total number of nucleations, $\mathbf{N_o}$ with $[Cl^-]$, (Table 3) is consistent with the availability of more potential sites for pit nucleation becoming accessible to activation. The increase in $\boldsymbol{\tau}$ may be associated with the activation of sites, which were not available at a lower $[Cl^-]$ at the same **E,** or at the same $[Cl^-]$ at different **E (**Table 4**)**. Such inaccessibility could have been due to compositional (reactivity) or geometrical (degree of site occlusion) difference of the inclusions.

The decay of the number of events as a function of size (Figures 6, 8 and 11) implies that the largest events are the rarest. It is expected that the tendency for a metastable pit to propagate from a nucleation would increase as the event gets bigger. More Cl^- will accumulate at the site as the nucleation size increases, making repassivation more difficult, and increasing the chances of metastable pit formation. Evidence to support the above argument is found in Figure 12, which is the height distribution of nucleations in deaerated 0.1MHCl at 0.2V(SCE) on SS316GF that propagated into metastable pits. It shows that the propensity to generate metastable pits increases with the size of the nucleation.

The occurrence of metastable pits is a rarity compared with the number of nucleations that occur (Tables 3 and 4). The increase in $\mathbf{N_o}$ as **E** and $[Cl^-]$ increase (Tables 3 and 4)

can be explained by the increase in the number of sites accessible to pit nucleation and the increase in tendency to accumulate Cl^- ions at sites of pit nucleation at a faster rate as **E** and $[Cl^-]$ increase. The implication is that more open sites can result in the propagation of metastable pits. It is not fully understood why τ for metastable pitting increases as **E** and $[Cl^-]$ increase. A possible reason may be that the additional sites that have been nucleated require more time for the accumulation of sufficient Cl^- for metastability to set in. If a site is more open, it is reasonable to expect that because of a reduced barrier to diffusion than a more occluded site, the time required to propagate the pit will be longer since more time will be needed to build up the required $[Cl^-]$. This might also explain the insignificant changes in the value of λ_o.

The reason for the reduction in the percentage of metastable pits that propagated from nucleations (although real number increased, Table 3) as $[Cl^-]$ increases and the insignificant change in percentage propagation as **E** increased (Table 4) is not fully understood. It could be expected that the number of metastable pits generated would be proportional to the number of nucleations that occur. The reduction in percentage of propagation as $[Cl^-]$ increased suggests that the proportion of nucleations that attained metastability decreased. A possible reason may be connected to the value of τ for nucleations as a function of $[Cl^-]$ and **E** (Tables 3 and 4). The increase in the value of τ as $[Cl^-]$ and **E** increase suggests that some of the events are difficult to nucleate. It may then be expected that metastable pits may even be more difficult to propagate from these events. This will therefore result in the repassivation of most of these events at the nucleation stage, resulting in the general reduction in percentage of metastable pits that were generated.

The effect of factors like the grain size (in this case determined by manufacturing process) and inclusion size on nucleation and metastable pitting were sought in this study. Since pits are usually nucleated at sites of non-metallic inclusions [15-17], it was expected that 316Com would be more active than SS316GF in Cl^- solution, since no inclusions were detected on SS316GF, but some measuring between 1 and 3 μm were detected on 316Com.

The higher values of λ_o and N_o obtained for nucleation and metastable pits for SS316GF compared with 316Com (Table 5) is believed to be a direct function of the number of nucleation sites on the surface of the metal. This suggests more numerous sites (inclusions) were present on SS316GF than on 316Com, and that they eluded detection because they were less than 1μm in diameter, the maximum resolution of SEM-EDX system used for analyses. The behavior of SS316GF may then be linked to the characteristics (size, number per cm^2, and perhaps the chemical reactivity) of the inclusions on the metal surface.

The more numerous sites on SS316GF may have been caused by the drawing process used in preparing the wires (used in the as-received state) which has the tendency not only of reducing the grain size of the specimen, but also the inclusion size by breaking them down into smaller aggregates, resulting in an increase in the number of potential pit nuclei. Since no inclusions were observed on this metal, the inclusions must have been lower than the resolution of the SEM used which was ~1μm. In the case of 316Com, the wires used for the experiment were prepared out of flat sheets by cutting out 0.1 x 0.1 x

18 cm portions for electropolishing without any cold working, resulting in the maintenance of the grain structure and inclusion size and distribution of the material. SEM showed some inclusions (albeit very few) on 316Com of between 1 and 3µm across, and it is possible that smaller inclusions were present on the metal surface that could not be detected. Since the surface area of the sample (316Com) used for the investigation was minute (3.2×10^{-4} to 3.9×10^{-4} cm^2) compared with the rest of the specimen (3.0×10^4 cm^2), it is believed that because of this, the number of inclusion in the microelectrode was very small and the probability that some of the large inclusions were present in the electrode even smaller. This may have led to the lower value of λ_o and N_o for 316Com. This is consistent with the finding that fewer number of nucleation sites (controlled by electrode size) result in higher measured pitting potentials [10].

Further evidence that the number of large inclusions on the 316Com electrode were very few (if present) may be found in Figure 11, which shows the height distribution of the events on both metals. A higher percentage and hence more nucleations occurred at much higher current ranges on SS316GF than on 316Com. This might suggests that 316Com had a higher proportion of smaller inclusions on its surface compared with SS316GF. The implication of this is that more metastable pits will be formed on SS316GF because the propensity to propagate them increases with the size of the nucleations (Figure 12). This explains why more metastable pits occurred on SS316GF than on 316Com. It could not be verified that 316Com was more resistant to stable pitting than SS316GF since both metals did not pit below or at 0.8V(SCE), the maximum potential employed in this study.

CONCLUSION

a) Increase in $[Cl^-]$ increased the initial frequency of nucleation λ_o, time constant, τ, and total number of nucleation events N_o. For metastable pitting, the increase in $[Cl^-]$ increased the time constant, τ, and total number of metastable pits N_o. λ_o the initial frequency of metastable pitting remained unaffected.
b) An increase in **E** increased the initial frequency of nucleation λ_o, and total number of nucleation events N_o. The time constant, τ, was unaffected. For metastable pitting, time constant, τ, and total number of metsatable pits N_o increased, while λ_o the initial frequency of metastable pitting was unaffected.
c) The number of these events decay exponentially with time in a manner consistent with first order kinetics.
d) The height distribution of events was unaffected by neither $[Cl^-]$ or **E**.
e) Metastable pits are difficult to propagate from nucleations. The propensity to generate them increases as the size of the nucleations increase. .
f) SS316GF had higher λ_o and N_o compared with 316Com for nucleations and metastable pits. SS316GF also nucleated a higher proportion of large events compared with 316Com. This suggests that SS316GF is more susceptible to pitting corrosion than 316Com.

This work was performed under the auspices of the U. S. Department of Energy by University of California, Lawrence Livermore National Laboratory under contract No. W-7405-Eng-48.

REFERENCES

1. W. Schwenk, Corrosion, **20**, 129t (1964).
2. H.H. Uhlig and J.R. Gilman, Corrosion, **20**, 289t (1964).
3. H.P. Leckie and H.H. Uhlig, J. Electrochem. Soc., **113**, 1262, (1966).
4. H.C. Man and D.R.Gabe, Corrosion Science, **21**, 713 (1981).
5. P.C. Pistorius and G.T. Burstein, Phil. Trans. R. Soc. Lond. **A341**, 531, (1992)
6. G.S. Frankel, L. Stockert, F. Hunkeler and H. Bohni, Corrosion, **43**, 429, (1987)
7. G.T. Burstein and S.P. Mattin, Phil. Mag. Lett., **66**, 127, (1992)
8. G.T. Burstein and S.P. Mattin, Phil. Mag. Lett., **76**, 341, (1997)
9. G.T.Burstein and G. O. Ilevbare, Corrosion Science, **43**, 485, (2001)
10. G.T.Burstein and G. O. Ilevbare, Corrosion Science, **38**, 2257, (1996)
11. G.T. Burstein and P.I. Marshall, Corrosion Science, **23**, 125, (1983)
12. G.T. Burstein and G.W. Ashley Corrosion, **40**,110, (1984)
13. G.T Burstein and A.J. Davenport,J. Electrochem. Soc. **136**, 936 (1989)
14. Handbook of chemistry and physics, 57th ed., R.C. Weast, Editor, pp. B85-B178, CRC press Cleveland OH (1976).
15. E.F.M. Jensen, W.G. Sloof and J.H.W. De Wit, in Modifications of Passive Films, P. Marcus, B. Baroux and M Keddam, Editors, p. 290, The Institute of Materials, London (1994).
16. A. Szummer, M. Janik-Czachor, and S. Hoffman, in Modifications of Passive Films, P. Marcus, B. Baroux and M Keddam, Editors, p. 280, The Institute of Materials, London (1994).
17. M.A. Baker and J.E. Castle, Corrosion Science, **34**, 667 (1993).

Table 1. Composition of SS316GF in wt%.

Cr	Ni	Mn	Mo	Si
19.4	11.8	2.2	2.4	0.2

Table 2. Composition of 316Com in wt%

S	Mn	Cr	Mo	Ni	P	Si	Cu	Nb	Ti	N	C	O
.008	1.69	16.9	2.55	11.7	.029	.36	.29	.01	.02	.04	.05	.004

Table 3. The time constant τ, initial frequency of events λ_o total number of events N_o, the running sum N_S for nucleations (a) and metastable pits (b) in deaerated 0.025MHCl + 0.075M$HClO_4$, 0.05MHCl + 0.05M$HClO_4$, 0.075MHCl + 0.025M$HClO_4$ and 0.1MHCl on SS316GF at 0.2V (SCE). R: regression coefficient.

Electrolytes	Nucleations				Metastable pits			
	τ/s	$\lambda_o/s^{-1}cm^{-2}$	$10^{-6}N_o/cm^{-2}$	R	τ/s	$\lambda_o/s^{-1}cm^{-2}$	$10^{-6}N_o/cm^{-2}$	R
0.025MHCl + 0.075M$HClO_4$	632	875	0.55	0.83	826	134	0.11	0.75
0.05MHCl + 0.05M$HClO_4$	1286	1348	1.73	0.74	1159	118	0.14	0.71
0.075MHCl + 0.025M$HClO_4$	939	2487	2.34	0.92	1591	129	0.21	0.66
0.1MHCl	1152	4441	5.12	0.94	1530	105	0.16	0.76

Table 4. The time constant τ, initial frequency of events λ_o, and total the number of events N_o per cm^2 in deaerated 0.025MHCl + 0.075M$HClO_4$. Polarization: 0.2V, 0.3 and 0.5V(SCE) on SS316GF. R: regression coefficient.

E/(SCE)	Nucleations				Metastable pits			
	τ/s	$\lambda_o/s^{-1}cm^{-2}$	$10^{-6}N_o/cm^{-2}$	R	τ/s	$\lambda_o/s^{-1}cm^{-2}$	$10^{-6}N_o/cm^{-2}$	R
0.2V	632	875	0.55	0.83	826	134	0.11	0.76
0.3V	754	2254	1.70	0.93	559	227	0.14	0.92
0.5V	633	3540	2.24	0.91	1550	108	0.35	0.76

Table 5. The time constant τ, initial frequency of events λ_o, and the total number of events N_o in deaerated 0.025MHCl + 0.075M$HClO_4$, on 316Com and SS316GF.

Metal	Nucleations				Metastable pits			
	τ/s	$\lambda_o/s^{-1}cm^{-2}$	$10^{-6}N_o/cm^{-2}$	R	τ/s	$\lambda_o/s^{-1}cm^{-2}$	$10^{-6}N_o/cm^{-2}$	R
316Com	2762	53	0.15	0.89	2135	7	0.01	0.77
SS316GF	685	451	0.31	0.76	826	134	0.11	0.90

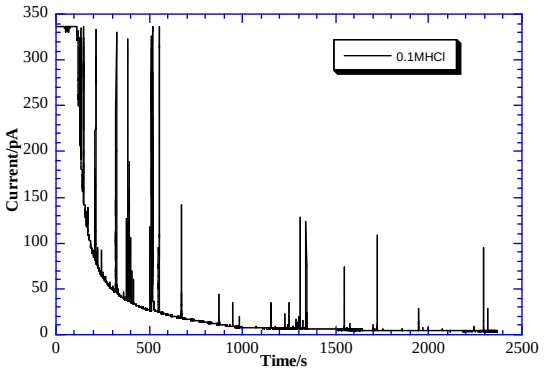

Figure 1. Current transient of SS316G in 0.1 M HCl for 2370s at 0.2V(SCE).

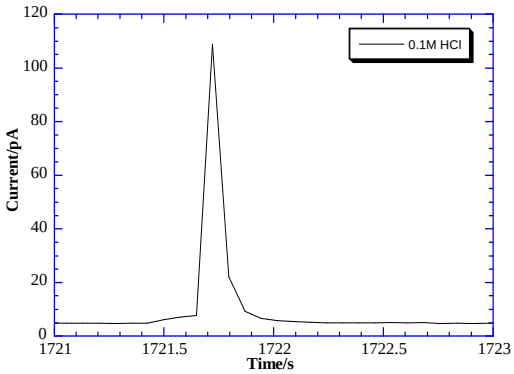

Figure 2. Current transients of single nucleation event on SS316G in 0.1MHCl at 0.2V(SCE). The height of this one is about 105pA.

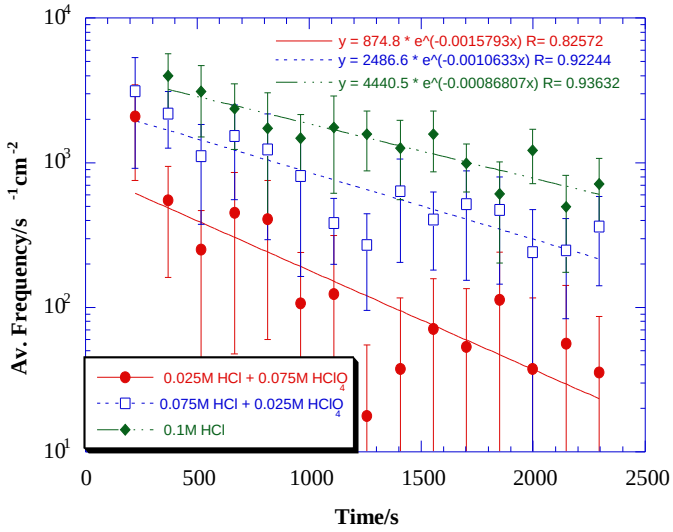

Figure 3. Average frequency of nucleations per cm^2 as a function of time in deaerated 0.025MHCl + 0.075M$HClO_4$, 0.075MHCl + 0.025M$HClO_4$ and 0.1MHCl on SS316GF at 0.2V (SCE).

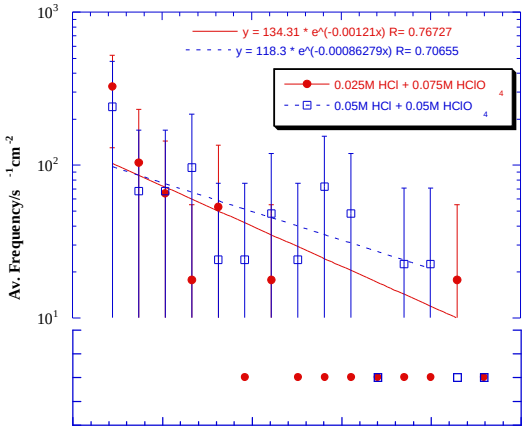

Figure 4. Average frequency of metastable events per cm^2 as a function of time in deaerated 0.025MHCl + 0.075M$HClO_4$, 0.05MHCl + 0.05M$HClO_4$, at 0.2 VSCE

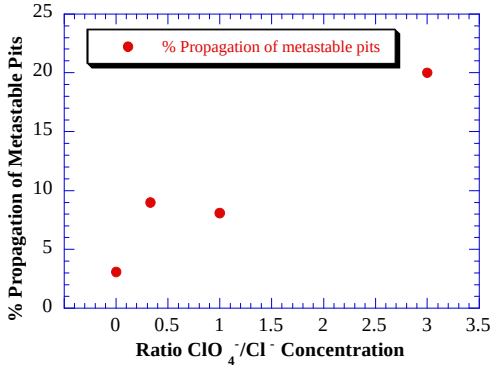

Figure 5. Percentage propagation of metastable pits as a function of $[ClO_4^-]/[Cl^-]$ ratio for SS316GF ad 0.2 V SCE

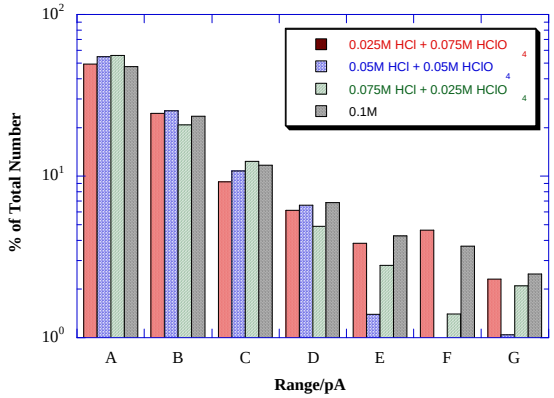

Figure 6. Peak current (height) distribution of nucleation events in deaerated 0.025MHCl + 0.075M$HClO_4$, 0.05MHCl + 0.05M$HClO_4$, 0.075MHCl + 0.025M$HClO_4$ and 0.1MHCl on SS316GF. Polarization: 0.2V(SCE) for 2370s.

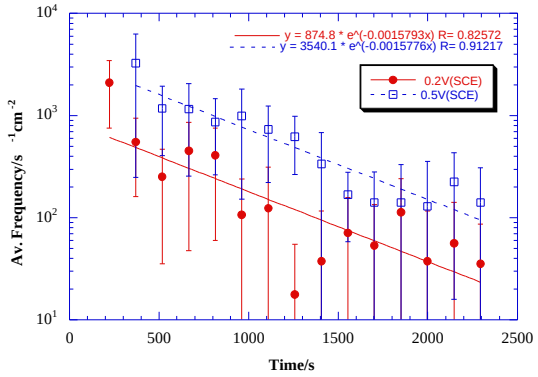

Figure 7. Average frequency of nucleations per cm^2 as a function of time in deaerated 0.025MHCl + 0.075$MHClO_4$ at 0.2V and 0.5V(SCE) on SS316GF.

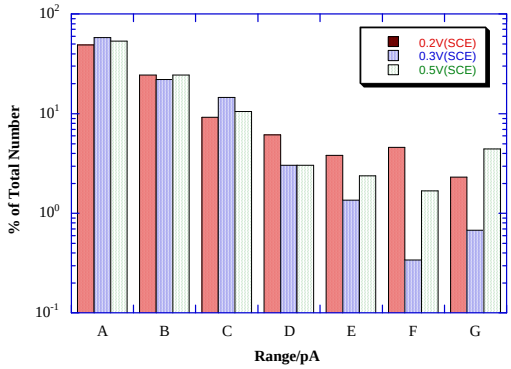

Figure 8. Height distribution of nucleation events in deaerated 0.025MHCl + 0.075$MHClO_4$ at 0.2V, 0.3 and 0.5V(SCE) on SS316GF.

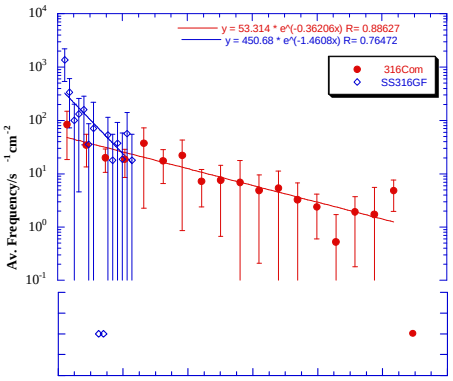

Figure 9. Average frequency of nucleation events per cm^2 as a function of time in deaerated 0.025MHCl + 0.075$MHClO_4$, on 316Com and SS316GF.

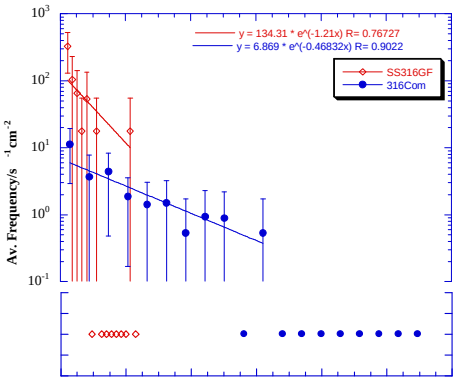

Figure 10. Average frequency of metastable events per cm^2 as a function of time in deaerated 0.025MHCl + 0.075$MHClO_4$, on 316Com and SS316GF.

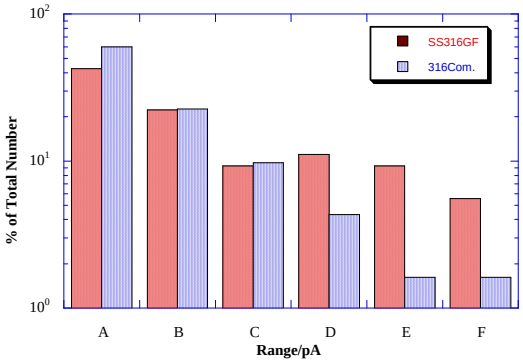

Figure 11. Height distribution of nucleation events in deaerated 0.025MHCl + 0.075$MHClO_4$ on 316Com and SS316GF at 0.2V(SCE).

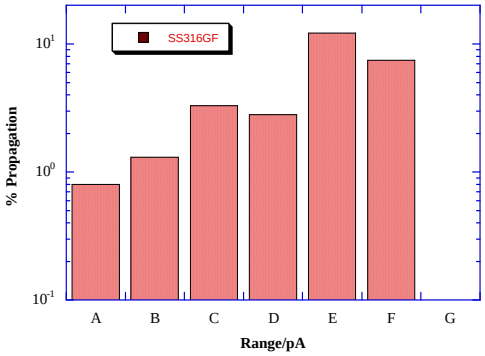

Figure 12. Height distribution of the total number of nucleations in deaerated 0.1MHCl at 0.2V(SCE) on SS316GF, which propagated into metastable pits. This graph was generated from a total of 22 metastable pits.

Keywords: Alloy 22, welds, gas tungsten arc weld (GTAW), localized corrosion, inhibition, corrosion potential, repassivation potential, cyclic polarization, nitrate, chloride, temperature.